Chaos and anomalous diffusion of ballistic electrons in lateral surface superlattices

J. Wagenhuber* and T. Geisel

Institut für Theoretische Physik (SFB Nichtlineare Dynamik), Universität Frankfurt,
D-6000 Frankfurt/Main, Federal Republic of Germany
and Institut für Theoretische Physik, Universität Regensburg, D-8400 Regensburg, Federal Republic of Germany

P. Niebauer and G. Obermair

Institut für Festkörperphysik, Universität Regensburg, D-8400 Regensburg, Federal Republic of Germany
(Received 20 May 1991; revised manuscript received 23 September 1991)

We study the classical dynamics of a charged particle in a two-dimensional (2D) lattice-periodic potential with a perpendicular magnetic field. Due to chaotic scattering the particle shows diffusion in 1D and 2D, as well as anomalous diffusion associated with $1/f$ noise. The onset of diffusion is explained by heteroclinic intersections and stochastic layers, and the transition from 1D to 2D diffusion is caused by the destruction of a separating Kolmogorov-Arnold-Moser torus. As a simplification we introduce a discrete-time model based on a separatrix map, which facilitates the analysis of free-path distributions related to the occurrence of anomalous diffusion. These results represent classical approximations for the dynamics of electron wave packets in lateral surface superlattices on semiconductor heterojunctions.

I. INTRODUCTION

Bloch electrons in the presence of a homogeneous magnetic field show a variety of interesting phenomena. Based on the Peierls-Onsager hypothesis, Hofstadter elucidated the existence of a self-similar band structure depending on the incommensurability of two characteristic length scales.[1,2] The corresponding quasiperiodic Schrödinger operator may have a spectrum with a singular continuous component and the wave functions may be critical or exotic, i.e., neither extended nor localized.[3] Quantum-mechanical wave packets spread diffusively without bound, i.e., their width increases linearly in time.[4] To circumvent unaccessibly strong magnetic fields Hofstadter suggested studying artificial two-dimensional (2D) superlattices with much larger lattice spacing than in natural crystals.[1] As the superlattice spacing is increased with respect to the Fermi wavelength; however, the dynamics of a wave packet approaches the classical limit. Today it is possible to realize high-mobility heterojunctions with lateral surface superlattices, and therefore the time has come to also investigate the classical counterpart of the problem, e.g., as an approximation for the dynamics of a ballistic electron.

In the present article we show that the classical counterpart of the problem studied by Hofstadter and others[1-5] exhibits chaotic behavior as the magnetic field causes a nonintegrable coupling between the two degrees of freedom, and we point out the relevance of Kolmogorov-Arnold-Moser (KAM) theory[6] for the observed phenomena. We investigate various types of chaotic diffusion and characterize them by a power spectral analysis of the current fluctuations. As the magnetic field is increased from zero, a one-dimensional (1D) anomalous diffusion process sets in. It is accompanied by $1/f$ noise corresponding to a nonlinear growth of the mean-square displacement. For strongest fields there are

transitions to 1D normal diffusion, 2D normal diffusion, and 2D anomalous diffusion. Based on Poincaré surfaces of section we explain the mechanism for the onset of 1D diffusion by the generation of stochastic layers due to heteroclinic intersections near the unperturbed separatrices. The transition to 2D diffusion is caused by the breakup of invariant KAM tori into cantori. We introduce a discrete-time model related to the whisker map to describe the diffusion mechanisms and the dynamics in the stochastic layers. Depending on a nonintegrability parameter, which is directly related to the magnetic field, the map generates normal and anomalous diffusion processes as well as transitions between these types of motion. While some of the occurring phenomena were outlined already in a previous Letter,[7] the discrete model now enables us to a closer analysis of the dynamics.[8]

As mentioned above, the most important application of the model is the motion of ballistic electrons in lateral surface superlattices (LSSL) on semiconductor heterojunctions.[9-12] At present these systems are studied intensely, not only for academic reasons but also for their potential use in future devices. The superlattice serves to break the lateral free-electron behavior and to produce minigaps.[9] Lateral superlattices with 1D modulations[10,11] and 2D modulations[12] have been realized with lattice parameters down to about 200 nm. The lattice parameter a is larger than the Fermi wavelength (e.g., $a/\lambda_F \approx 8$ in Ref. 10) and it is a problem to reduce this ratio rather than to increase it. The dynamics of wave packets can therefore be treated on the basis of classical approximations.[13] Strictly speaking, the classical equations of motion result from a quasiclassical treatment of the superlattice potential for the dynamics of quantum wave packets in k space. In the effective-mass approximation for the band structure, which is valid in III-V-compound semiconductors, the quasiclassical equations of motion reduce to the classical equations of a

Hamiltonian system with a mass determined by the effective mass m^* and a total energy determined by the Fermi energy E_F.

For a typical 2D modulating potential we have previously studied the classical chaotic dynamics in the absence of a magnetic field.[14,15] We found a mechanism for $1/f$ noise and presented a statistical theory for its explanation. Avoiding the chaotic dynamics would require a special modulating potential consisting of two perpendicular plane waves. This situation may be realized, e.g., using the persistent photoconductivity effect.[10] Considering such an integrable potential we show here, however, that addition of a magnetic field will again cause chaotic behavior. One of our conclusions regards the elastic mean free path l_e (~ 10 μm in $Al_{1-x}Ga_xAs/GaAs$ heterojunctions[10]). The occurrence of chaotic diffusion in a regular superlattice may reduce the lengths of free paths. Other possible applications of this classical treatment are related to particle channeling, fast ion conductors, and electrostatic plasma waves.

The article is organized as follows. The model and its equations of motion are introduced in Sec. II. Dynamical and statistical properties are investigated in Sec. III and explained in terms of KAM theory and heteroclinic intersections. Section IV reduces the dynamics to a discrete map and relates its statistical behavior to the charge-carrier diffusion.

II. CLASSICAL MODEL OF BALLISTIC DYNAMICS

A. Equations of motion

We consider a classical particle with charge e moving in a two-dimensional superlattice potential under the influence of a perpendicular homogeneous magnetic field $\mathbf{B} = B\hat{\mathbf{z}}$ along the z axis, as described by the Hamiltonian

$$H(x,y,p_x,p_y) = \frac{1}{2m}\left[\left(p_x + \frac{eB}{2}y\right)^2 + \left(p_y - \frac{eB}{2}x\right)^2\right] + V(x,y) . \quad (2.1)$$

We assume the simplest case of an isotropic potential in two dimensions with superlattice constant a

$$V(x,y) = V_0\left[2 + \cos\left(\frac{2\pi}{a}x\right) + \cos\left(\frac{2\pi}{a}y\right)\right] . \quad (2.2)$$

Measuring energy and length in units of the potential strength and the superlattice constant, respectively, we obtain scaled variables

$$\tilde{H} = \frac{H}{V_0}, \quad \tilde{x} = \frac{2\pi}{a}x, \quad \tilde{y} = \frac{2\pi}{a}y, \quad \tilde{t} = \omega_0 t . \quad (2.3)$$

Time is measured in units of the inverse harmonic frequency

$$\omega_0 = \frac{2\pi}{a}\left[\frac{V_0}{m}\right]^{1/2} \quad (2.4)$$

which arises in the quadratic approximation of the super-

lattice potential. The equations of motion then read (omitting the tildes for convenience)

$$\dot{x} = v_x, \quad \dot{v}_x = \sin x + 2\lambda v_y , $$
$$\dot{y} = v_y, \quad \dot{v}_y = \sin y - 2\lambda v_x , \quad (2.5)$$

corresponding to the Hamiltonian

$$H(x,y,p_x,p_y) = \tfrac{1}{2}(p_x + \lambda y)^2 + \tfrac{1}{2}(p_y - \lambda x)^2 + V(x,y) \quad (2.6)$$

with a scaled potential

$$V(x,y) = 2 + \cos + \cos y . \quad (2.7)$$

The dimensionless quantity

$$\lambda = \frac{eB}{\sqrt{mV_0}}\frac{a}{4\pi} = \frac{\omega_c}{2\omega_0} \quad (2.8)$$

proportional to the applied magnetic field B describes the nonintegrable coupling between the two degrees of freedom and is related to the bare cyclotron frequency. Concerning the magnetic field λ there are two integrable limits in this model, that is, $\lambda \to 0$ (electrostatic limit) and $\lambda \to \infty$ (magnetic limit). In lateral surface superlattices this parameter can easily be varied in a large range, as it does not only depend on B, but is also inversely proportional to $V_0^{1/2}$. Very small potential amplitudes $V_0 \leq 1$ meV are obtained by the persistent photoconductivity effect,[10] whereas for lithographically patterned gates V_0 can be varied between 0 and 1 eV by tuning the gate voltage.[11,12] It is thus easy to reach values of λ between 10^{-3} and 10^1 (e.g., $\lambda = 4$ for $V_0 = 1$ meV, $B = 1$ T, and $a = 1\mu$m).

B. Energy regimes

The equations of motion in Eq. (2.5) are canonical and therefore the total energy $E \equiv H$ of the system is conserved. The two parameters E and λ determine the physical situation. The potential V in Eq. (2.7) has minima at the energy $E = 0$, saddle points at $E = 2$, and maxima at $E = 4$. Depending on the total energy E we distinguish three energy regimes. In the *low energy regime* $E < 2$, all orbits are localized within one unit cell of the potential for all values of λ. For *intermediate energies* $2 < E < 4$, drifting quasiperiodic orbits extended in x but not in y, and vice versa, may coexist with localized orbits in dependence of λ. At *high energies* $E > 4$, possible orbits are in principle not restricted in configuration space. The most interesting phenomena, deterministic diffusive motion and $1/f$ noise, occur in the intermediate energy regime, with which the main part of this work is concerned.

III. NUMERICAL RESULTS

A. Power spectrum and transport properties

We have analyzed the particle motion by means of the velocity power spectrum

$$S_\alpha(\omega) = \frac{1}{2\pi}\int_{-\infty}^{\infty} \langle v_\alpha(t)v_\alpha(0)\rangle e^{i\omega t}dt , \quad (3.1)$$

where α distinguishes the Cartesian components. In Eq. (3.1) the angular brackets denote time averaging, so that the power spectrum appears as a Fourier transform of the velocity autocorrelation function. This relation, together with the well-known equation[16]

$$\sigma_\alpha^2(t) = 2 \int_0^t (t - s) \langle v_\alpha(s) v_\alpha(0) \rangle ds \qquad (3.2)$$

from the theory of stochastic processes, gives rise to interdependence between the low-frequency behavior of the power spectrum $S_\alpha(\omega)$ and the asymptotic behavior of the mean-square displacement $\sigma_\alpha^2(t) = \langle \Delta\alpha^2(t) \rangle$ for $t \to \infty$. As described in previous articles,[14] two varieties of diffusive motions may occur in classical models for ballistic electron dynamics.

Normal diffusion is characterized by a linear growth of the mean-square displacement with time $\sigma_\alpha^2(t) \sim 2Dt$, while the power spectrum $S_\alpha(\omega)$ converges to a finite limit for $\omega \to 0$. The diffusion coefficient $D = \pi S_\alpha(\omega = 0)$ is finite.

Anomalous diffusion is related to a nonlinear growth $\sigma_\alpha^2(t) \sim t^{1+\beta}$ with $0 < \beta \le 1$ of the mean-square displacement and a low-frequency divergence $S_\alpha(\omega) \sim \omega^{-\beta}$ of the spectral density. Our numerical results exhibit cases with $\beta \approx 1$, i.e., with an occurrence of $1/f$ noise in the spectral density $S(\omega)$ of the velocity fluctuations.

If there is *no transport* at all in a particular direction (x or y) the corresponding power spectrum (S_x or S_y) vanishes in the low-frequency limit. This occurs in the low-energy regime $E < 2$, where all orbits remain confined to one lattice cell.

We have determined power spectra $S_\alpha(\omega)$ in the intermediate regime $2 < E < 4$. Qualitatively, the results do not vary strongly with the actual value of the total energy E. Therefore we present the main numerical results for a special choice $E = 2.92$ (Figs. 1 and 2) and others for $E = 3.82$ (Fig. 3). The numerical determination of the power spectra makes use of the Wiener-Khinchin theorem[16]

$$S_\alpha(\omega) = \frac{1}{2\pi} \left| \int_{-\infty}^{\infty} v_\alpha(t) e^{i\omega t} dt \right|^2 \qquad (3.3)$$

and circumvents the determination of the autocorrelation function. Using a set of initial conditions located in the stochastic layers [see, e.g., Fig. 8(a)] we have obtained the following results.

At total energy $E = 2.92$ and with increasing magnetic field λ starting from $\lambda = 10^{-4}$ the velocity fluctuations show $1/f$ noise $S_y(\omega) \sim \omega^{-\beta}$ in the low-frequency limit with $\beta \approx 1$ [Fig. 1, spectrum (a)] up to fields $\lambda \le 10^{-3}$. As described above, this behavior of the power spectrum is associated with anomalous diffusion $\langle \Delta y^2(t) \rangle \sim t^{1+\beta}$. Note that the diffusive motion is only in one dimension, the direction (x or y) being determined by the initial conditions. In our special choice the motion is diffusive along the y axis and is localized in the x direction. The corresponding power spectrum $S_x(\omega)$ vanishes at low frequencies. Due to the fourfold rotational symmetry of our model we can also prepare initial conditions with diffusive motion in the x direction and localization in the y direction. In this case we achieve the same results as
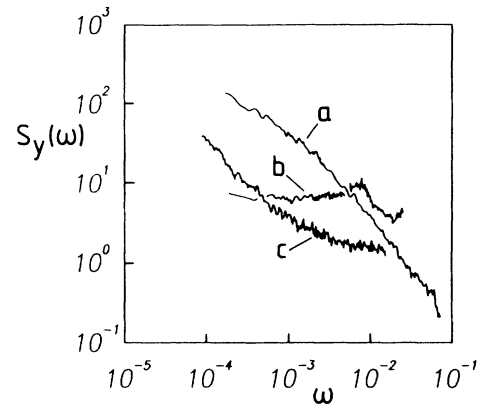

FIG. 1. Velocity power spectra $S_y(\omega)$ for various magnetic-field strengths λ at total energy $E = 2.92$. Frequency is in units of the harmonic frequency ω_0. For (a) $\lambda = 10^{-3}$ and (c) $\lambda = 0.07$, $S_y(\omega)$ diverges as $\omega^{-\beta}$ with $\beta \approx 1$ corresponding to anomalous diffusion. For (b) $\lambda = 10^{-2}$, $S_y(\omega)$ remains finite as $\omega \to 0$ corresponding to normal diffusion.

above. As we increase the magnetic field, we find a transition region above $\lambda = 10^{-3}$ where the character of the spectrum changes. Near $\lambda = 10^{-2}$ the low-frequency divergence has disappeared [Fig. 1, spectrum (b)]. We can thus conclude that there is a transition to normal diffusion characterized by a finite value of the diffusion coefficient $D = \pi S_y(0)$ and by a linear growth of the mean-square displacement $\langle \Delta y^2(t) \rangle$. So far, however, the normal diffusion remains one dimensional. At a critical field strength $\lambda_c \approx 0.014$ we found a transition from 1D diffusion to 2D diffusion where the particle performs a random walk in the x-y plane. Both power spectral densities $S_x(\omega)$ and $S_y(\omega)$ have a finite limit for $\omega \to 0$. With increasing values of λ the 2D diffusion also becomes anomalous [Fig. 1, spectrum (c) and Fig. 2, spectrum (d)], as $S_x(\omega)$ and $S_y(\omega)$ exhibit $1/f$ noise. Normal diffusion in 2D is reached again above $\lambda \approx 0.3$ [Fig. 2, spectrum (e)], whereas above $\lambda \approx 0.5$ all orbits are localized within
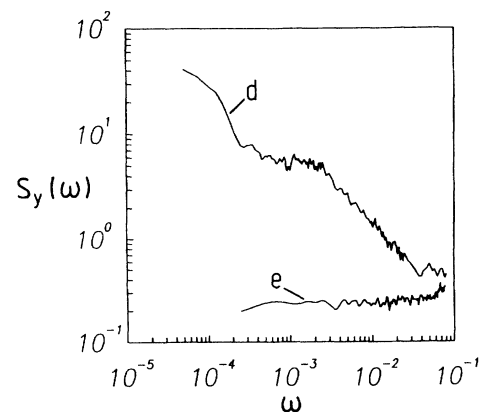

FIG. 2. Same as Fig. 1 with different values of the magnetic-field strength λ. For (d) $\lambda = 0.12$, $S_y(\omega) \sim \omega^{-\beta}$ (with $\beta \approx 1$) pertaining to anomalous diffusion. For (e) $\lambda = 0.3$, $S_y(\omega)$ remains finite for $\omega \to 0$ corresponding to normal diffusion again.

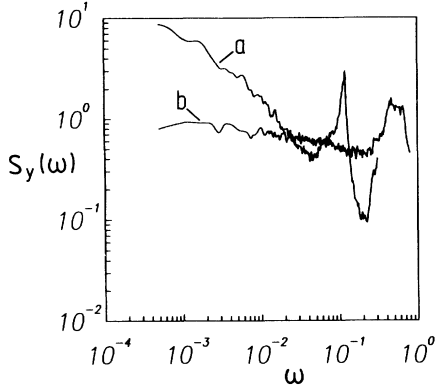FIG. 3. Velocity power spectra for various magnetic-field strengths λ at total energy $E = 3.82$. For (a) $\lambda = 8 \times 10^{-4}$, $S_y(\omega)$ diverges as $\omega^{-\beta}$ ($\beta \approx 1$) corresponding to anomalous diffusion, which is one dimensional here. For (b) $\lambda = 0.25$, $S_y(\omega)$ converges to a finite limit as $\omega \to 0$. Diffusion is normal and now two dimensional.

one unit cell of the potential. This localization is related to the value of the cyclotron radius, which for

$$\lambda > \frac{1}{\pi} \left[\frac{E}{2} \right]^{1/2} \tag{3.4}$$

becomes smaller than the superlattice constant. For a different total energy $E = 3.82$ one finds the same scenario, although the critical λ values for the transitions are different (Fig. 3).

B. Distribution of free-path lengths

We have verified the above conclusions concerning the transport properties in the intermediate energy regime by studying the distribution of free paths, which are easily discerned in the motion of the particle. Free paths are motions crossing the boundaries of one or more lattice cells. For chaotic diffusion in a perfectly ordered potential, free paths are intermittent, i.e., they start and end in chaotic motions within a cell. The chaotic dynamics gives rise to a quasirandom scattering of ballistic electrons. Thus we assume successive paths as statistically independent and describe the distributions of their lengths by a probability density $\psi_\alpha(\ell)$, where $\psi_\alpha(\ell) d\ell$ equals the fraction of paths parallel to the α axis with lengths between ℓ and $\ell + d\ell$. For computational reasons and in order to get better statistics we determine the integrated probability distribution

$$\Phi_\alpha(\ell) = \int_\ell^\infty \psi_\alpha(\ell') d\ell' . \tag{3.5}$$

For obvious reasons the asymptotic behavior of the distribution of free paths is related to the type of transport in the system. Also, there is an interdependence between the power spectrum $S_\alpha(\omega)$ and the probability density $\Phi_\alpha(\ell)$.

Suppose that we have a single ballistic path of duration τ_L. As long as $t \leq \tau_L$ the contribution of this single path to the velocity autocorrelation function $C(t)$ is propor-

tional to the length of an interval in which a correlation between time τ and time $\tau + t$ is possible, i.e.,

$$C(t) \propto \langle v^2 \rangle (\tau_L - t) . \tag{3.6}$$

For an ensemble of statistically independent free paths we only need to sum up contributions of individual free paths and the autocorrelation function becomes

$$C_\alpha(t) = \frac{\langle v_\alpha^2 \rangle}{\langle \ell \rangle} \int_\ell^\infty (\ell' - \ell) \psi_\alpha(\ell') d\ell' . \tag{3.7}$$

Here we have transformed from the duration of free paths to their length $\ell = t \sqrt{\langle v^2 \rangle}$ using a mean-squared velocity $\langle v^2 \rangle$. The average length $\langle \ell \rangle$ of ballistic paths gives the correct normalization in Eq. (3.7). In order to get a relationship between the probability density $\psi_\alpha(\ell)$ and the power spectrum we return to the definition Eq. (3.1). The velocity autocorrelation is an even function and thus

$$S_\alpha(\omega) = \frac{1}{\pi} \int_0^\infty C_\alpha(t) \cos(\omega t) dt . \tag{3.8}$$

Performing a partial integration and observing that the autocorrelation vanishes for physical reasons as $t \to \infty$, we obtain

$$S_\alpha(\omega) = -\frac{1}{\pi \omega} \int_0^\infty C_\alpha'(t) \sin(\omega t) dt . \tag{3.9}$$

According to Eq. (3.7)

$$\begin{aligned} C_\alpha'(t) &= \frac{d\ell}{dt} \frac{dC}{d\ell}(t) \\ &= -\frac{\langle v_\alpha^2 \rangle^{3/2}}{\langle \ell \rangle} \int_\ell^\infty \psi_\alpha(\ell') d\ell' \\ &= -\frac{\langle v_\alpha^2 \rangle^{3/2}}{\langle \ell \rangle} \Phi_\alpha(\ell) . \end{aligned} \tag{3.10}$$

Equations (3.9) and (3.10) combine to a relation connecting the velocity power spectrum with the integrated probability density of free path lengths[8]

$$S_\alpha(\omega) = \frac{\langle v_\alpha^2 \rangle}{\pi \langle \ell \rangle \omega} \int_0^\infty \Phi_\alpha(\ell) \sin \left[\frac{\omega \ell}{\sqrt{\langle v_\alpha^2 \rangle}} \right] d\ell . \tag{3.11}$$

Using Eq. (3.11) we can now relate the behavior of the free-path distribution to the various types of transport, which we observe in the classical model of ballistic electron motion. *Normal diffusion* is implied by an exponential decay $\Phi_\alpha(\ell) \sim e^{-a\ell}$ of the integrated free-path distribution, since in this case the power spectrum becomes a Lorentzian

$$S_\alpha(\omega) \sim \frac{1}{\omega^2 + a^2} , \tag{3.12}$$

which yields a finite value for the diffusion coefficient $D = \pi S_\alpha(0)$. In the case of *anomalous diffusion* we find algebraically decaying long-time tails $\Phi_\alpha(\ell) \sim \ell^{-\nu}$ in the integrated distribution of free paths. For $\nu < 2$, Eq. (3.11) then yields $S_\alpha(\omega) \sim \omega^{-\beta}$, where

$$\nu + \beta = 2 . \tag{3.13}$$

Numerically we have obtained the integrated distribution $\Phi_\alpha(\ell)$ of free paths independent of Eq. (3.11). Their length is given by the number of successive cell boundary crossings. Their distribution was determined by counting their occurrence in the course of time. All cases of normal diffusion were connected with exponentially decaying free path distributions [e.g., Fig. 4(a)], while the cases of enhanced anomalous diffusion were accompanied by long-time tails $\Phi_\alpha(\ell) \sim \ell^{-\nu}$ (for large ℓ) in the free-path distribution mostly with $\nu \approx 1$ [e.g., Fig. 4(b)]. According to Eq. (3.13) this implies $\beta \approx 1$, i.e., $1/f$ noise in the current fluctuations. In Sec. IV we will construct a discrete dynamical system, in which all these features of the free-path distribution are recovered. It thus can serve as a model for investigating chaotic diffusion and transitions between various types of diffusive motion in nonintegrable Hamiltonian systems.

C. Poincaré surfaces of section

The mechanisms leading to the different types of diffusion can be understood by analyzing Poincaré surfaces of section (Figs. 5–10). In all cases we plot the in-
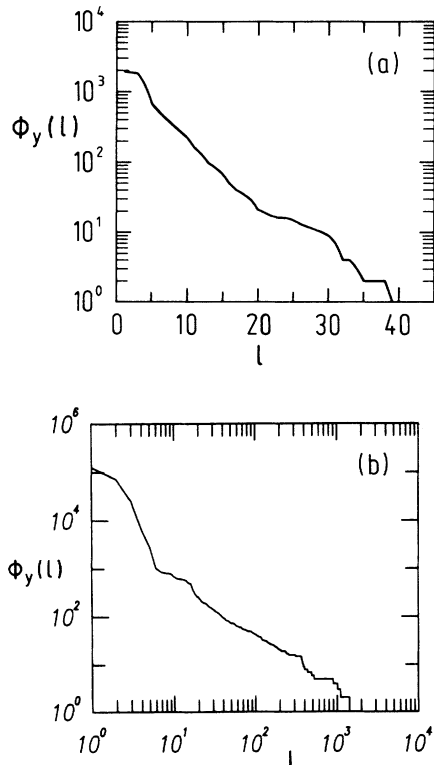

FIG. 4. (a) Integrated probability distribution $\Phi_y(\ell)$ (unnormalized) of free-path lengths at total energy $E = 2.92$ and magnetic-field strength $\lambda = 0.01$. The distribution $\Phi_y(\ell)$ falls off exponentially as $\ell \to \infty$ implying normal diffusion. (b) Same as (a) for magnetic-field strength $\lambda = 0.07$. The distribution decays algebraically as $\Phi_y(\ell) \sim \ell^{-\nu}$ for $\ell \to \infty$ with $\nu \approx 1$. This corresponds to anomalous diffusion and $1/f$ noise in the velocity power spectrum.
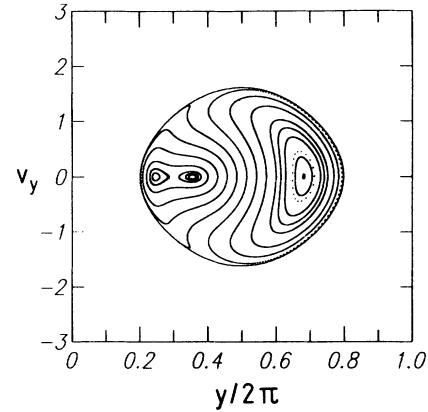

FIG. 5. Poincaré surface of section at the potential minimum for total energy $E = 1.3$ and magnetic field $\lambda = 0.1$. The motion appears regular.

tersections of phase-space orbits with the y-v_y plane at $x = \pi$ (mod2π), i.e., at the potential minima. Due to the discrete translational symmetry of the superlattice potential we identify all y coordinates $mod\,2\pi$ and thus reduce them to the unit cell $[0, 2\pi]$. The phase-space trajectory is uniquely determined by the points in the surface of section. We can partition the total energy as $E = E_x + E_y$, where E_x and E_y are the instantaneous energies in each degree of freedom, e.g., $E_y = 1 + \cos y + v_y^2/2$. Since E_x and E_y are positive definite, the outer boundary of the Poincaré surfaces of section is always given by the curve $E_y = E$. In the case of low energies $E < 2$ this curve is closed, implying that in this situation the particle is confined within one unit cell. For intermediate and high energies $(E > 2)$ the boundary consists of two separate curves and transport across superlattice cells is possible. Because of the fourfold rotational symmetry of the lattice it suffices to consider only Poincaré sections in the y-v_y plane as they are identical with the x-v_x sections. Another choice for Poincaré surfaces of section would be in the y-v_y plane at $x = 0$ (mod2π), i.e., at the saddle points of the potential.[14] This choice, however, would not display localized pieces of the phase-space trajectory and thus is not suitable in the present context.
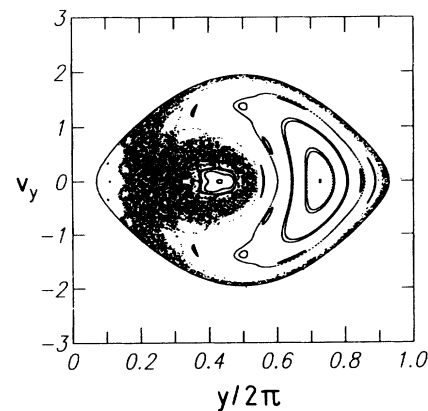

FIG. 6. Poincaré surface of section at the potential minimum for $E = 1.9$ and $\lambda = 0.1$. A stochastic layer has grown and now covers a noticeable part of the phase space.
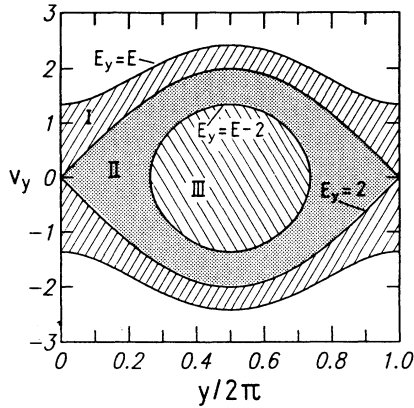
FIG. 7. Poincaré surface of section at the potential minimum for intermediate energies with $2 < E < 4$ (here $E = 2.92$) as it appears in the zero-field case (i.e., $\lambda = 0$). Two separatrices divide the phase space into regions of delocalized (drifting) motions (III) and localized orbits (II).

FIG. 8. (a) Poincaré surface of section at the potential minimum for intermediate energy $E = 2.92$ and magnetic field $\lambda = 0.01$. The onset of diffusive motion is related to the creation of stochastic layers around the two separatrices caused by heteroclinic intersections. (b) Partial magnification of (a). KAM tori in the region of localized orbits (Fig. 7, region II) separate the two stochastic layers and therefore diffusion is one dimensional.
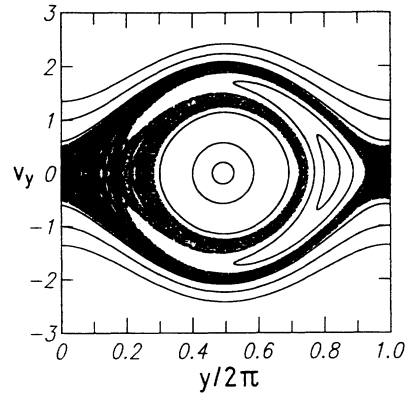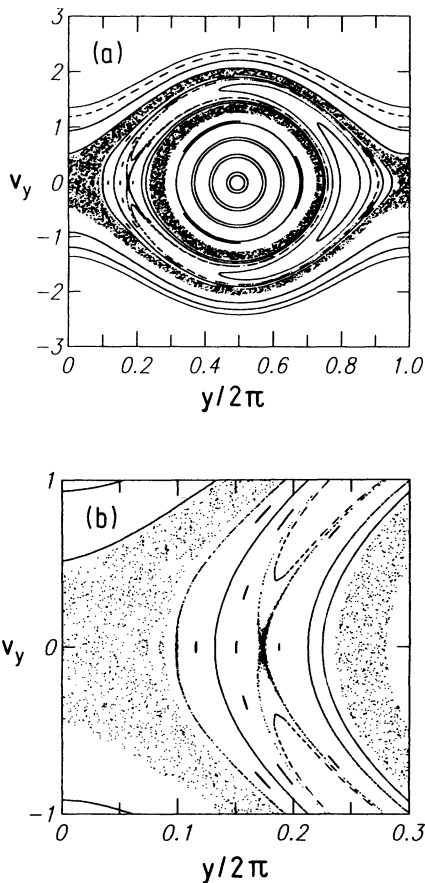

FIG. 9. Same as Fig. 8 for $\lambda = 0.014$. Two-dimensional diffusion sets in as the KAM tori separating the two stochastic layers in Fig. 8 are destroyed. The connected stochastic region was generated by a single orbit.

1. Low-energy regime

In a first part we consider Poincaré surfaces of section for energies $E < 2$ (Figs. 5 and 6). We have obtained surfaces of section for magnetic fields in the range from $\lambda = 0.001$ to 0.1 and for energies between $E = 1.3$ and 1.9. Chaotic behavior becomes important for magnetic fields $\lambda \gtrsim 0.1$. While for energies $E \lesssim 1$ the Poincaré surfaces of section show regular motions (Fig. 5), for higher energy a region of stochastic motion appears in the vicinity of a hyperbolic fixed point. The size of this stochastic region grows with increasing energy (Fig. 6).

The regular motions for $E \lesssim 1$ can be understood by partitioning the superlattice potential

$$V(x,y) = V_c(r) + \Delta V(x,y) \tag{3.14}$$

in a point symmetric part

$$V_c(r) = 2 - 2J_0(r) \tag{3.15}$$

with $r^2 = x^2 + y^2$ and a perturbation ΔV, which breaks the continuous rotational symmetry. If $\Delta V \equiv 0$ there is another invariant of motion besides the total energy E,
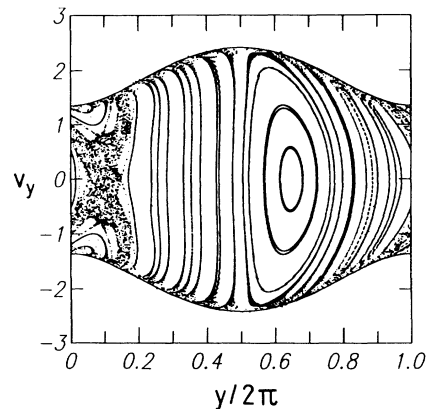

FIG. 10. Same as Fig. 8 for $\lambda = 1.0$. In the limit of strong magnetic fields the stochastic region is shrinking and a regime of regular (localized) motion is reached again.

the z component L_z of the angular momentum. The Hamiltonian system then is integrable, allowing only regular orbits in phase space. As long as $E \lesssim 1$, the perturbation ΔV is small and does not substantially alter the regular motions in the surface of section (e.g., Fig. 5). Higher energies involve stronger perturbations ΔV and give rise to the occurrence of chaotic dynamics (Fig. 6). In the low-energy regime, the energy E thus serves as a parameter controlling the transition from regular to chaotic dynamics, in contrast to the case of intermediate energies (see below). This transition to chaos is of interest in itself. In the following we will concentrate, however, on large-scale chaotic motions occurring above $E = 2$.

2. Intermediate-energy regime

A detailed analysis of Poincaré surfaces of section done at intermediate energies shows that the magnetic field λ is the relevant parameter affecting the dynamics and the transport properties (see Figs. 1–3). We have determined surfaces of section for various energies $2 < E < 4$ and various field parameters from $\lambda = 10^{-4}$ to about $\lambda = 2$ [Figs. 8(a)–10]. Consider first the zero-field case $\lambda = 0$ (Fig. 7). Here the Hamiltonian (2.6) separates into Hamiltonians for two uncoupled pendula as can be seen in the decoupling of the equations of motion (2.5). The energies E_x and E_y of the x and y degrees of freedom are each conserved. The Hamiltonian system is integrable and regular orbits appear as invariant curves of constant E_y in the surfaces of section. The sections thus look similar to the phase portrait of a pendulum. There are two pendulum separatrices, however, for $E_y = 2$ and $E_y = E - 2$ (i.e., where $E_x = 2$), which divide the plane into three regions as shown in Fig. 7: In region I, above the y separatrix $(E_y > 2)$, the orbits correspond to running solutions of the y pendulum. They correspond to delocalized motion in the y direction (drifting orbits) and must be localized in x (in the intermediate-energy regime $2 < E < 4$). In region III, for $E_y < E - 2$, we have $E_x > 2$, and therefore the orbits belong to running solutions of the x pendulum and localized motion in the y direction. Note that these two regions are interchanged under the symmetry operation $x \mapsto y$, $y \mapsto -x$ ($\pi/2$ rotation). In the intermediate region II, we have $E_y < 2$ and $E_x < 2$ corresponding to swinging motion of both pendula. The particle thus remains confined in both directions within one unit cell. The area II of localized orbits between the two separatrices decreases with increasing total energy and disappears for $E \geq 4$, when the particle energy exceeds the potential maximum. In the surface of section there is an elliptic fixed point at $y = \pi, v_y = 0$, corresponding to the minimum of the potential, and a hyperbolic point at $y = 0, v_y = 0$, corresponding to the saddle point of the potential V. As we apply a magnetic field ($\lambda > 0$), regular drifting orbits continue to exist in regions I and III [Fig. 8(a)] in accordance with the KAM theorem.[6] Around each of the two separatrices a *stochastic layer* is generated, in which the orbits perform irregular chaotic dynamics [Fig. 8(a)]. These stochastic layers exist for the lowest fields ($\lambda \leq 10^{-4}$), although they are only visible under

sufficiently strong magnification. They extend into the regions of localized (II) and delocalized (I or III) orbits (see Fig. 7) and thus a chaotic orbit in the layer can switch in a finite time from a localized region to a delocalized region and vice versa. This is the origin of diffusive motion in 1D. The layer around the outer separatrix generates diffusion in the y direction. For symmetry reasons the inner layer plays the same role for the x direction. The stochastic layers and thus the onset of 1D diffusion are caused by heteroclinic intersections of the unstable and stable manifolds[6] of the hyperbolic fixed point at $y = 0, v_y = 0$. In the next section we approximate the dynamics in the stochastic layer responsible for 1D diffusion by a discrete map.

The mechanism for transition from 1D diffusion to 2D diffusion can be understood from a magnification of Fig. 8(a) shown in Fig. 8(b). We can clearly distinguish KAM tori in the region II of localized orbits separating the inner and outer stochastic layer. Since KAM tori are invariant manifolds, they cannot be penetrated by chaotic orbits. An orbit in the outer layer thus cannot reach the inner layer and a particle diffusing in the y direction cannot change to a free path in the x direction and vice versa. For this reason, diffusion is possible only in 1D as long as these KAM tori are not destroyed by increasing resonances. In Fig. 8(a) we also distinguish a pair of elliptic and hyperbolic fixed points in the localized region II, resulting from a 1:1 nonlinear resonance with rotation number $\alpha_y = \omega_y / \omega_x = 1$. For $\lambda = 0$ this rotation number belongs to an invariant curve with $E_y = E_x = E/2$. The KAM tori outside this curve have $E_y > E_x$ and therefore $\alpha_y < 1$; the ones inside have $\alpha_y > 1$. The most prominent KAM tori in these regions have golden-mean rotation number $\alpha_y = \gamma = (\sqrt{5} + 1)/2$ and $\alpha_y = 1/\gamma = \gamma - 1$. These are the most irrational rotation numbers in the sense of a continued fraction expansion. The golden tori are the most robust as they are far from resonant conditions and are the last to be destroyed. This happens at a critical field of $\lambda_c \simeq 0.014$ where the inner and outer layers start being connected (Fig. 9) and can both be visited by individual orbits in the course of time. Diffusion in two dimensions is thus generated for fields $\lambda \geq \lambda_c$. The rate of switching between x diffusion and y diffusion is determined by the flux across the two golden cantori (broken tori). From work on the standard map[17] we may expect that it shows critical scaling behavior near λ_c with a power-law growth as $(\lambda - \lambda_c)^{3.011722}$.

In Fig. 9 the elliptic fixed point at the center $y = \pi, v_y = 0$ (for $\lambda = 0$, see Fig. 7) moves to the left according to the Lorentz force, which also points left for $v_x > 0$. Similarly the KAM tori in region III are not centered at $y = \pi, v_y = 0$ but are shifted to the left to an extent depending on the mean value of v_x, or the diameter of the circles. The hyperbolic point at $y = 0, v_y = 0$ (for $\lambda = 0$), however, moves to the right due to the Lorentz force and the local y curvature of the potential at the saddle point, which is opposite to the y curvature in the minimum.

For still larger values of the magnetic field $\lambda \geq 1.0$ the stochastic region shrinks again and regular motion predominates (Fig. 10). This is because for

$$\lambda \gg \frac{1}{\sqrt{8E}} \tag{3.16}$$

the force due to the potential can be neglected with respect to the magnetic force. In the magnetic limit the particle performs regular motions localized in one unit cell. In this section we have only presented Poincaré surfaces of section for $E = 2.92$. Surfaces of section for other energy values in the intermediate regime are qualitatively similar[8] and are therefore not included in this paper. For example, for $E = 3.82$ (Fig. 3) we find the same scenario as above. The main difference consists in other critical values λ for the transitions between different types of diffusion. So for $E = 3.82$ the transition to 2D diffusion occurs at lower values of λ as the localized region II shrinks with increasing energy. The magnetic limit according to Eq. (3.16) is also reached at smaller fields.

IV. DISCRETE MODEL OF DIFFUSION

In the preceding section we gave a qualitative explanation for the occurrence of anomalous diffusive motion and $1/f$ noise in the velocity power spectrum. It was shown that diffusion is caused by the growth of a *stochastic layer* near the unperturbed separatrix. In the present section we will construct a discrete map for the dynamics in the stochastic layer. Relating the diffusion process to the iteration of a separatrix map[18] will reproduce all features of diffusive motion in the system including transitions between various types of diffusion.

To construct this discrete map we consider the outer stochastic layer at the unperturbed separatrix $E_y = 2$ [see, e.g., Fig. 8(a)], i.e., we treat the case where the y degree of freedom switches between localized and delocalized motions for $E_y \approx 2$. For reasons of symmetry the inner stochastic layer is described by the same map. At first sight one might expect that the applicability of the separatrix map is restricted to small values of λ, where the y pendulum stays near the outer separatrix and diffusion is in 1D, as the stochastic layers are not connected. Our numerical investigations will show, however, that transitions between normal and anomalous diffusion also occur in the regime of 2D motion. This is due to the fourfold rotational symmetry of the Hamiltonian system, where the stochastic layers and corresponding separatrices can be interchanged by a symmetry operation. The same map (although with a different meaning of the energy variable w) describes all the dynamics of scattering processes occurring within each of the stochastic layers.

For $E \approx 2$ the motion of the y pendulum depends sensitively on the momentary value of E_y. For $E_y > 2$ the pendulum rotates, whereas for $E_y < 2$ it shows oscillations. We consider in detail the motion of the pendulum in the time interval T_y, defined to enclose a full rotation in the case $E_y > 2$ and *half* of an oscillation for $E_y < 2$. The length of this time interval in the unperturbed case is given by

$$T_y = \begin{cases} 2K(k_y) & \text{for } E_y < 2 \\ 2K(k_y^{-1})/k_y & \text{for } E_y > 2 \end{cases} \tag{4.1}$$

where

$$k_y = \left[\frac{E_y}{2}\right]^{1/2} \tag{4.2}$$

is the *modulus* and K denotes a complete elliptic integral of the first kind. As the motion of the y pendulum is sensitive to $E_y < 2$ and $E_y > 2$ we introduce a new variable

$$w = E_y - 2 . \tag{4.3}$$

An expansion near $E_y = 2$, i.e., $k_y = 1$, yields the approximation[19]

$$T_y = \ln(32/|w|) . \tag{4.4}$$

Note that the duration of oscillation and rotation diverges logarithmically as the pendulum approaches the separatrix, i.e., as $w \to 0$.

While the y pendulum performs a rotation or half of an oscillation, the x pendulum oscillates because of the condition $E < 4$, i.e., $E_x < 2$. To a first approximation we regard the x pendulum as a driving force, acting on the motion in the y degree of freedom. We now determine the additive change Δw of the variable w within the time interval T_y for a typical motion of the y pendulum.

$$\Delta w = \Delta E_y = \int_{-T_y/2}^{T_y/2} \dot{E}_y \, dt . \tag{4.5}$$

Evaluation of the Poisson brackets for $E_y = v_y^2/2 + 1 + \cos y$ immediately gives

$$\dot{E}_y = \{E_y, H\} = \{E_y, E_x\} = -2\lambda v_x v_y . \tag{4.6}$$

This equation can be understood in terms of the Lorentz force in the y direction expressed by

$$dE_y/dy = -2\lambda v_x . \tag{4.7}$$

Equations (4.5) and (4.6) lead to

$$\Delta w = -2\lambda \int_{-T_y/2}^{T_y/2} v_x v_y \, dt . \tag{4.8}$$

In order to get an explicit expression for Eq. (4.8) we introduce the following approximations. We use the unperturbed swinging motion of the x pendulum as we set

$$v_x = 2k_x \text{cn}(t + \tau_0 | k_x) , \tag{4.9}$$

where cn denotes the Jacobian elliptic cosine and the variable τ_0 describes the phase difference between the motions of the x and y pendulum, respectively. We will see later that besides the energy variable w, the phase τ_0 is the second variable involved in the discrete description of the stochastic layer dynamics. As a further approximation we replace the motion of the y pendulum, which is near the outer separatrix by the unperturbed separatrix motion

$$v_y(t) = 2/\cosh(t) . \tag{4.10}$$

As a consequence we then set the lower and upper limits of the integral in Eq. (4.8) to infinity,

$$\Delta w = -8\lambda k_x \int_{-\infty}^{\infty} \frac{\mathrm{cn}(t+\tau_0|k_x)}{\cosh(t)} dt \ . \tag{4.11}$$

The Jacobian elliptic cosine can be expanded in a Fourier series[19]

$$\mathrm{cn}(u|k_x) = \frac{2\omega_x}{k_x} \sum_{n=0}^{\infty} \frac{\cos[(2n+1)\omega_x u\,]}{\cosh[(2n+1)\omega_x K(\sqrt{1-k_x^2})]} \ . \tag{4.12}$$

Carrying out the integral in Eq. (4.11) we obtain Δw as an infinite series

$$\Delta w = -16\lambda\pi\omega_x \sum_{n=0}^{\infty} \frac{\cos[(2n+1)\omega_x\tau_0]}{\cosh[(2n+1)\omega_x K(\sqrt{1-k_x^2})]\cosh[(2n+1)\omega_x\pi/2]} \ , \tag{4.13}$$

where ω_x denotes the frequency of the swinging x pendulum. In the investigated energy range $E < 3$, the coefficients of the infinite series fall off very rapidly (by a factor of about 500 between the first two coefficients) and thus a good approximation is given by the first term of the sum

$$\Delta w = -\frac{16\lambda w_x\pi\cos(\omega_x\tau_0)}{\cosh[\omega_x K(\sqrt{1-k_x^2})]\cosh(\omega_x\pi/2)} \ . \tag{4.14}$$

As far as the energy variable w is concerned, the dynamical structure of the stochastic layer is described by the map

$$\bar{w} = w + \Delta w \ . \tag{4.15}$$

Besides, also the phase of the swinging x pendulum is mapped to a new value. It changes additively by the duration T_y of the y motion

$$\bar{\tau}_0 = \tau_0 + T_y \ . \tag{4.16}$$

For convenience we replace $\omega_x\tau_0$ by τ_0 and obtain the map

$$\bar{w} = w - \Lambda\cos(\tau_0) \ ,$$
$$\bar{\tau}_0 = \tau_0 + \omega_x\ln(32/|w|) \ , \tag{4.17}$$

where according to Eq. (4.14)

$$\Lambda \approx 10\lambda \text{ and } \omega_x < 1 \tag{4.18}$$

in the parameter region considered here.

The map in Eqs. (4.17) is not canonical and does not preserve the phase-space volume in (w,τ_0). A canonical form of Eqs. (4.17) can be obtained by computing the phase shift T_y [Eq. (4.4)] from the final energy $\bar{w}$,

$$\bar{w} = w - \Lambda\cos(\tau_0) \ ,$$
$$\bar{\tau}_0 = \tau_0 + \Omega\ln(32/|\bar{w}|) \ . \tag{4.19}$$

The map is now area preserving and it is an example for Chirikov's whisker map.[18] To make a connection to Ref. 18, ω_x used in Eqs. (4.17) is replaced by Ω. We want to emphasize that in our model Ω is restricted to $[0,1]$ due to the physical meaning of ω_x.

We now relate the dynamics of the separatrix map to the particle diffusion in the system. According to Eq.

(4.3), for $w < 0$ the y pendulum performs a swinging motion ($E_y < 2$). The electron is therefore momentarily localized in one unit cell along the y direction. In the case $w > 0$, however, the electron performs a delocalized, ballistic motion in the y direction corresponding to rotations for the y pendulum ($E_y > 2$). This implies that a sequence of positive values of w occurring in the iteration of the map belongs to a ballistic free path (see Sec. III B) over a number of lattice cells corresponding to the length of the sequence. By iteration of the map Eq. (4.19) we can thus deduce the statistic distribution of free-path length from a discrete model of the stochastic layer dynamics. We may expect that at least the 1D diffusive motion can be described and that different types of diffusion (normal and anomalous) can be distinguished in that way. Note that a backscattering process is connected with a change of the phase $\bar{\tau}_0 = \tau_0 + n\pi$ where n is odd, whereas forward scattering belongs to even values of n.

We have studied the temporal behavior of the discrete model Eq. (4.19). Detection of sequences with positive values of the variable w as described above and counting the various free path lengths (i.e., the length of sequences $w > 0$) directly gives the (unnormalized) integrated distribution $\Phi(\ell)$ [see Eq. (3.5)]. In order to remove singularity effects we have used an ensemble of initial conditions from which the iterations are started.

Figures 11 and 12 show the integrated distribution $\Phi(\ell)$ obtained from Eq. (4.19) for a constant frequency $\Omega = 1$ and for various "magnetic-field strengths" from $\Lambda = 10^{-3}$ to 1. For weak magnetic fields $\Lambda \leq 10^{-2}$ we found an algebraic decay $\Phi(\ell) \sim \ell^{-\nu}$ of free-path lengths with $\nu \approx 1$ [see Fig. 11, distribution (a), $\Lambda = 10^{-2}$]. As we have shown in Sec. III, this pertains to anomalous diffusion and to a low-frequency divergence $S(\omega) \sim \omega^{-\beta}$ with $\beta \approx 1$ in the velocity power spectrum. The same result is recovered for strong fields $\Lambda \geq 1.0$ [see Fig. 11, distribution (c), $\Lambda = 1.0$]. At intermediate values, however, a transition to an exponential decay $\Phi(\ell) \sim e^{-a\ell}$ of free path lengths and hence to normal diffusive motion with a Lorentzian power spectrum is observed (Fig. 12, $\Lambda = 0.05$).

In between the critical values of the magnetic field corresponding to normal and anomalous diffusion there is a regime where the decay for large ℓ follows another power law $\Phi(\ell) \sim \ell^{-\nu}$ with $\nu \approx 2$ [Fig. 11, distribution (b), $\Lambda = 0.1$]. It can be shown[20] from Eqs. (3.2), (3.7), and
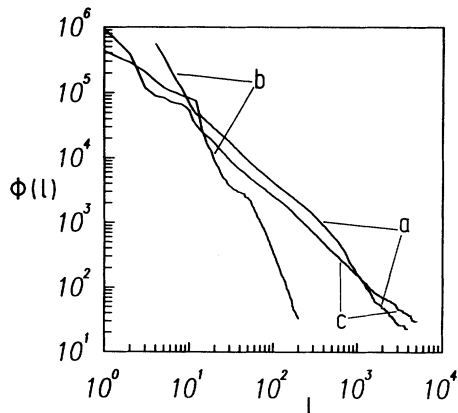
FIG. 11. Integrated probability distribution $\Phi(\ell)$ of free-path lengths (unnormalized) resulting from the separatrix map Eq. (4.19) for (a) $\Lambda=0.01$, (b) $\Lambda=0.1$, (c) $\Lambda=1.0$. The length of ballistic paths falls off algebraically like $\Phi(\ell)\sim\ell^{-\nu}$ with (a) $\nu\approx1$, (b) $\nu=2$, (c) $\nu\approx1$.

(3.8) that in the case $\nu=2$ the power spectrum diverges logarithmically $S(\omega)\sim|\ln\omega|$ and the mean-square displacement $\sigma^2(t)$ diverges like $t\ln t$, i.e., diffusion is anomalous by a logarithmic correction only. We point out that this intermediate regime of quadratic decay $\Phi(\ell)\sim\ell^{-2}$ for $\ell\to\infty$ of the distribution reproduces an analogous regime in the original Hamiltonian system [Eqs. (2.6) and (2.7)], which also shows up in between the critical values of the magnetic field λ corresponding to normal and anomalous diffusion (see, e.g., Fig. 13 for $\lambda=0.04$). As the separatrix map has a universal applicability in nonintegrable Hamiltonian systems, this might be a universal transition regime between normal and anomalous temporal behavior. Also from a formal point of view the case $\nu=2$ represents a transition point from anomalous to normal diffusion as the exponent ν of algebraic distributions $\Phi(\ell)\sim\ell^{-\nu}$ crosses the value $\nu=2$ from below. Algebraic distributions, although with a different exponent ν, have previously been reported for the whisker map in a different parameter regime.[21] In that work the parameter Λ was fixed ($\Lambda=1$), while the frequency ratio Ω was varied from $\Omega=1$ to 100. This rather applies to a fast driven nonlinear pendulum under strong perturbation.
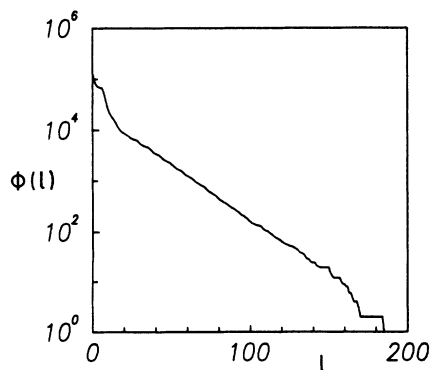

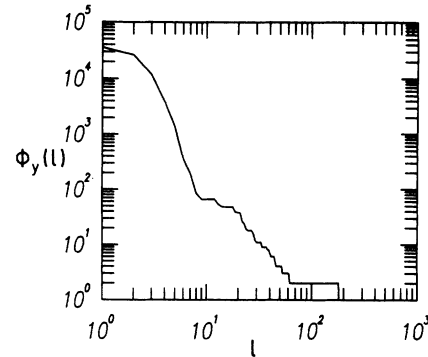FIG. 12. Same as Fig. 11 for $\Lambda=0.05$. $\Phi(\ell)$ decays exponentially.

FIG. 13. Integrated probability distribution $\Phi_y(\ell)$ of free-path lengths (unnormalized) of the original Hamiltonian system at total energy $E=2.92$ and $\lambda=0.04$. In this transition regime between normal and anomalous diffusion we find a quadratic decay $\Phi_y(\ell)\sim\ell^{-2}$ for $\ell\to\infty$ similar to the one found in the separatrix map model [see Fig. 11, distribution (b)].

In Ref. 14 an explanation for the occurrence of $1/f$ noise and anomalous diffusion was given in terms of a trapping mechanism in a hierarchy of nested barriers (cantori) in phase space. The hierarchy stems from the self-similar structure of nonlinear resonances in phase space manifesting themselves as islands of regular motion embedded in the chaotic sea. Each island contains KAM tori and is encircled by broken tori (cantori) acting as partial barriers. A chaotic orbit may penetrate into this infinite hierarchy of barriers and remain trapped for an arbitrarily long time. If the hierarchy dominates the delocalized regions of phase space (e.g., region I in Fig. 7) the particle can be trapped in long free paths and exhibit $1/f$ noise fluctuations.[14] In the framework of the separatrix map we expect a modification of this mechanism. If there is a hierarchy in the upper part ($w>0$) of its chaotic sea, trapping in this region may cause a long-time tail in the distribution $\Phi(\ell)$ of free paths. This is what we find, indeed, in the cases associated with $1/f$ noise. More exactly, whenever we found a distribution $\Phi(\ell)\sim\ell^{-1}$ there was a trapping hierarchy at the upper boundary of the chaotic sea, which could not be detected in the cases of exponential distributions $\Phi(\ell)\sim e^{-a\ell}$.

V. CONCLUSION

The main application of our work is to the motion of ballistic electrons in lateral surface superlattices (LSSL's). We predict that the chaotic dynamics in the anharmonic potential gives rise to diffusive scattering and thereby can lead to a finite mean free path or to a reduction of the mean free path of an experimental system. Depending on the parameters we do not only find regimes of normal diffusion with a linear growth of the mean-square displacement, but also regimes of anomalous diffusion with quadratic growth and associated $1/f$ noise in the velocity power spectrum. The speed of transport in the latter regime is thus comparable to a pure ballistic motion. In electronic devices where short switching times are required, an anomalous diffusive regime will show a better performance than a normal diffusive regime.

The mechanisms for the onset of different diffusive regimes were analyzed in detail. One-dimensional diffusion is caused by heteroclinic intersections of stable and unstable manifolds and the birth of a stochastic layer at the unperturbed separatrix. A transition from 1D to 2D diffusion arises by the destruction of the last separating KAM torus. Anomalous diffusion and $1/f$ noise is related to a trapping of chaotic orbits in a self-similar hierarchy of nested cantori. The analysis was facilitated by the introduction of a simplified discrete-time model, which makes use of a separatrix map. It reproduces various regimes and allows a more convenient analysis of free-path distributions.

The values of the coupling parameter λ considered here can be realized experimentally in LSSL's. As discussed in Sec. II A, the necessary values of the magnetic field and period of the superlattice are easily accessible (e.g., $\lambda=4$ for $B=1$ T, $a=1$ μm, and $V_0=1$ meV). In realistic samples there is an elastic mean free path ℓ_e due to scattering on impurities. It can be as large as 12 μm corresponding to more than 30 lattice cells.[10] The mean free path $\langle \ell \rangle$ associated with chaotic diffusion in the normal regimes is an order of magnitude below [e.g., $\langle \ell \rangle = 4.3$ unit cells in Fig. 4(a)]. Chaotic diffusion can thus lead to an observable reduction of the elastic mean free path. In antidot lattices a reduction from $\ell_e = 33$ unit cells to 2.4 unit cells was recently reported.[23] These samples are sufficiently clean that classical nonlinear orbits are reflected in magnetoresistance peaks.

The anomalous diffusive regimes will be harder to detect, of course. They are indicated by $1/f$ noise in the velocity power spectrum $S(\omega)$ as in Fig. 1. This quantity is directly accessible in experiments since the Kubo formula for the classical frequency-dependent conductivity $\sigma(\omega)$ and the definition of $S(\omega)$ [Eq. (3.1)] are proportional. Figures 1–3 for $S(\omega)$ thus also represent the conductivity $\sigma(\omega)$ (up to a prefactor), which can be measured in far-infrared (FIR) and microwave experiments. The onset of normal diffusion will be indicated by a non-vanishing low-frequency value $\sigma(\omega \rightarrow 0)$, i.e., dc conductivity, whereas anomalous diffusive regimes will be reflected by a power-law increase of $\sigma(\omega)$ as $\omega \rightarrow 0$. As a matter of fact, FIR transmission measurements on 2D periodic arrays of quantum dots have recently been reported by Lorke, Kotthaus, and Ploog.[22] Their results indeed display an increasing low-frequency background of $\sigma(\omega)$ as the gate voltage is varied from -3.1 to -2.7 V (Fig. 3) of Ref. 22). This may be a first indication for the onset of an anomalous diffusion process.

The power-law behavior of $S(\omega)$ and $\sigma(\omega)$ for the anomalous diffusive regimes is expected to hold down to infinitesimal frequencies ω in a perfectly pure system. The presence of impurities introduces a mean free time (which otherwise would be infinite) of the order of the time between collisions τ_{coll}. Correspondingly there will be a crossover frequency $\omega_{cr} \sim 1/\tau_{coll}$ where the power-law behavior ends and turns into a constant for $\omega < \omega_{cr}$. Very pure samples with mobilities above 1×10^6 cm^2/V sec can be realized today (e.g., Refs. 10 and 23), for which ω_{cr} is of the order of 3×10^{10} sec^{-1}. An upper limit of the power-law regime is given by the harmonic frequency $\omega_0 = (2\pi/a)(V_0/m)^{1/2}$ of the superlattice potential. For soft potentials, i.e., for sufficiently small V_0, the anomalous diffusive regime will thus be covered by impurity scattering. In harder potentials, however, which arise in antidot superlattices (considering a finite depletion length)[23] the upper limit ω_0 is shifted to higher frequencies. For example, for values of $V_0 = 100$ meV and $a = 0.2$ μm one has $\omega_0 = 2 \times 10^{13}$ sec^{-1} and thus the anomalous diffusion can show up in the FIR regime down to ω_{cr}. The impact of impurity scattering on the nonlinear dynamics is treated in more detail in a paper[24] on the interpretation of magnetoresistance experiments.

ACKNOWLEDGMENTS

*Permanent address: Siemens-Nixdorf Informationssysteme, Otto-Hahn-Ring 6, D-8000 München 83, Federal Republic of Germany.

[1]D. R. Hofstadter, Phys. Rev. B 14, 2239 (1976).

[2]For reviews see, e.g., B. Simon, Adv. Appl. Math. 3, 463 (1982); J. B. Sokoloff, Phys. Rep. 126, 189 (1985).

[3]S. Ostlund, and R. Pandit, Phys. Rev. B 29, 1394 (1984).

[4]T. Geisel, R. Ketzmerick, and G. Petschel, Phys. Rev. Lett. 66, 1651 (1991).

[5]G. Obermair, and H.-J. Schellnhuber, Phys. Rev. B 23, 5185 (1981); H.-J. Schellnhuber, G. Obermair, and A. Rauh, ibid. 23, 5191 (1981).

[6]See, e.g., M. V. Berry in Topics in Nonlinear Dynamics, AIP Conf. Proc. No. 46 edited by S. Jorna (American Institute of Physics, New York, 1978), p. 16 and D. F. Escande, Phys. Rep. 121, 163 (1985).

[7]T. Geisel, J. Wagenhuber, P. Niebauer, and G. Obermair, Phys. Rev. Lett. 64, 1581 (1990).

[8]J. Wagenhuber, Ph.D. thesis, Universität Regensburg, 1990.

[9]H. Sakaki, K. Wagatsuma, J. Hamasaki, and S. Saito, Thin Solid Films 36, 497 (1976); R. T. Bate, Bull. Am. Phys. Soc. 22, 407 (1977); A. C. Warren, D. A. Antoniadis, H. I. Smith, and J. Melngailis, IEEE Electron. Device Lett. ED-6, 294 (1985).

[10]R. R. Gerhardts, D. Weiss, and K. v. Klitzing, Phys. Rev. Lett. 62, 1173 (1989).

[11]R. W. Winkler, J. P. Kotthaus, and K. Ploog, Phys. Rev. Lett. 62, 1177 (1989).

[12]D. K. Ferry, G. Bernstein, and Wen-Ping Liu, in Physics and Technology of Submicron Structures, edited by H. Heinrich, G. Bauer, and F. Kuchar, Springer Series in Solid State Sciences Vol. 83 (Springer-Verlag, Berlin, 1988), p. 37; K. Ismail, W. Chu, A. Yen, D. A. Antoniadis, and H. I. Smith, Appl. Phys. Lett. 54, 460 (1989); P. H. Beton, E. S. Alves, M. Henini, L. Eaves, P. C. Main, O. H. Hughes, G. A. Toombs, S. P. Beaumont, and C. D. W. Wilkinson, J. Phys. Condens. Matter 1, 8257 (1989); A. Lorke, J. P. Kotthaus, and K. Ploog, Phys. Rev. Lett. 64, 2559 (1990); H. Fang and P. J.

Stiles, Phys. Rev. B **41**, 10 171 (1990); K. Ensslin and P. M. Petroff, *ibid.* **41**, 12 307 (1990); D. Weiss, M. L. Roukes, A. Menschig, P. Grambow, K. v. Klitzing, and G. Weimann, Phys. Rev. Lett. **66**, 2790 (1991).

[13]C. W. J. Beenakker, Phys. Rev. Lett. **62**, 2020 (1989); C. W. J. Beenakker, and H. van Houten, *ibid.* **63**, 1857 (1989).

[14]T. Geisel, A. Zacherl, and G. Radons, Phys. Rev. Lett. **59**, 2503 (1987); T. Geisel, A. Zacherl, and G. Radons, Z. Phys. B **71**, 117 (1988).

[15]A. Zacherl, T. Geisel, J. Nierwetberg, and G. Radons, Phys. Lett. **114A**, 317 (1986).

[16]See, e.g., F. Reif, *Fundamentals of Statistical and Thermal Physics* (McGraw-Hill, New York, 1965).

[17]R. S. MacKay, J. D. Meiss, and I. C. Percival, Physica D **13**, 55 (1984).

[18]B. V. Chirikov, Phys. Rep. **52**, 263 (1979).

[19]See, e.g., I. S. Gradshteyn and I. M. Ryzhik, *Table of Integrals, Series and Products* (Academic, New York, 1965), Nos. 8.113 and 8.146.

[20]T. Geisel, J. Nierwetberg, and A. Zacherl, Phys. Rev. Lett. **54**, 616 (1985).

[21]B. V. Chirikov and D. L. Shepelyansky, Physica D **13**, 395 (1984).

[22]A. Lorke, J. P. Kotthaus, and K. Ploog, Phys. Rev. Lett. **64**, 2559 (1990).

[23]D. Weiss, M. L. Roukes, A. Menschig, P. Grambow, K. v. Klitzing, and G. Weimann, Phys. Rev. Lett. **66**, 2790 (1991).

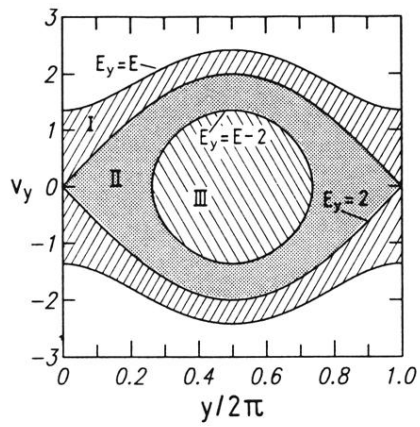[24]R. Fleischmann, T. Geisel, and R. Ketzmerick (unpublished).

FIG. 7. Poincaré surface of section at the potential minimum for intermediate energies with $2 < E < 4$ (here $E = 2.92$) as it appears in the zero-field case (i.e., $\lambda = 0$). Two separatrices divide the phase space into regions of delocalized (drifting) motions (III) and localized orbits (II).